
Proceedings Paper:
Terzioglu, F. orcid.org/0000-0002-2639-2992, Rongong, J. and Lord, C. (2022) Construction of motional phase maps for granular dampers. In: Proceedings of the 51st International Congress and Exposition on Noise Control Engineering (internoise2022). 51st International Congress and Exposition on Noise Control Engineering (Internoise 2022), 21 Aug - 24 Dec 2022, Glasgow, United Kingdom. Internoise , Glasgow, United Kingdom . ISBN 9781906913427

---

inter.noise
21-24 AUGUST
SCOTTISH EVENT CAMPUS
GLASGOW
2022

Construction of motional phase maps for granular dampers

Furkan Terzioglu[1]
Department of Mechanical Engineering, University of Sheffield
Mappin Street, Sheffield, S1 3JD, United Kingdom

Jem A. Rongong[2]
Department of Mechanical Engineering, University of Sheffield
Mappin Street, Sheffield, S1 3JD, United Kingdom

Charles E. Lord[3]
Department of Mechanical Engineering, University of Sheffield
Mappin Street, Sheffield, S1 3JD, United Kingdom

ABSTRACT

Harmonically vibrated granular media exhibit a variety of motional behaviours depending on amplitude, frequency, and vibration-to-gravity directional orientation. Motional behaviour defines the physical interactions of particles in the granular media and therefore the energy dissipation performance. A "phase map" that describes motional behaviour over broad ranges of frequency and amplitude is therefore a very useful tool in damper design. However, at present, identification of the operating motional conditions within the granular media has only been conducted by visual observation of the particles following a particle-level simulation or a specifically designed experiment. Because of this, design optimisation over a broad range of amplitude and frequency becomes costly. This paper aims to help reduce this cost through the development of approximate phase maps based on expected dissipative interactions of particles. Three-dimensional discrete element method simulations are conducted over a wide range of excitation intensities under two different vibration-to-gravity directional orientations (i.e., perpendicular, and parallel to the standard gravity direction) to allow the observation of as many motional phases as possible. The effect of particle size, volume filling ratio and particle shape on granular energy dissipation sources are also investigated.

1. INTRODUCTION

Granular dampers typically consist of relatively small particles packed inside a closed void. These devices are employed in the locations of a structure where the vibration levels are high. Such an approach can provide efficient dampening of structural vibrations (1) and reduction in noise levels (2). Granular damping performance is relatively insensitive to changes in working environment and material properties and is therefore especially desirable under challenging working conditions such as oily (3), cryogenic (4) and high temperature (5).

[1] fterzioglu1@sheffield.ac.uk

[2] j.a.rongong@sheffield.ac.uk

[3] c.lord@sheffield.ac.uk

Even though the conceptual design of a granular damper seems simple, it needs a specially planned design methodology to accomplish an effective energy dissipation as it shows non-linear behaviours (6–8). The amplitude and frequency dependent non-linear energy dissipation in granular dampers is attributed to the dynamic motional state (or phase) of damping particles in a vibration cycle since it determines the way that the particles interact with each other and surrounding boundaries (9,10). As an example, the non-linear energy dissipation effectiveness behaviour of a harmonically vibrated granular medium is shown in Figure 1 depending on frequency and amplitude. The different levels of energy dissipation effectiveness in this figure are the results of different motional phases observed in the granular medium (10).

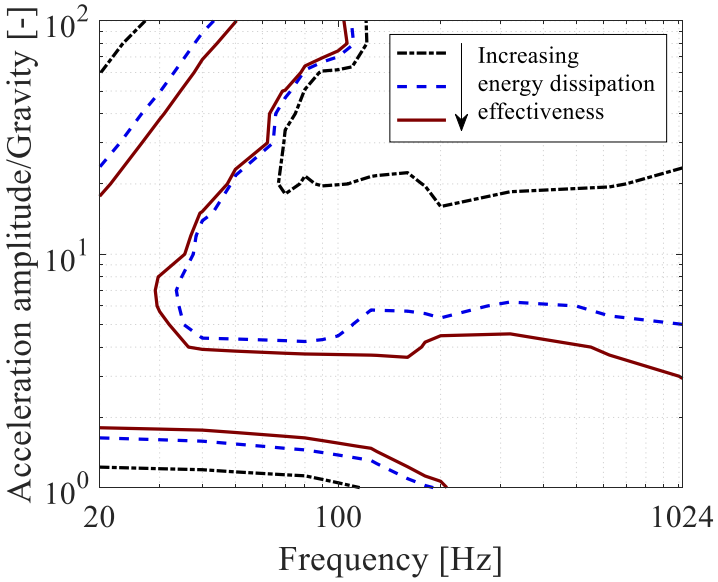

Figure 1: Energy dissipation effectiveness level of a granular damper depending on loading condition (10).

Depending on the dominant motion type that governs particle movements, the operating motional phase is identified at a given loading condition for a granular medium (11). As it can change with the loading condition, granular motional phase maps, on which the identified motional phases are shown in an amplitude-frequency plane, are considered useful for granular damper design (7,12). However, the derivation of motional phase maps requires time-consuming visual observations of simulations and experiments of a particulate system.

In this study, dissipative interactions were investigated using particle-level simulations for a granular damper experiencing different motional phases. This involved relating the energy dissipation behaviour of the damper to the dominant motional phase present under those particular conditions. The aim was to develop approximate motional phase maps without the need for time-intensive, visual analysis of data.

Section 2 describes the methodology and specific parameters used in the simulations. The relationship between the relative role of dissipative interaction types and the associated phase maps is discussed in Section 3. In Section 4, the most effective granular motional behaviours in terms of energy dissipation are briefly investigated. Finally, the conclusions are presented in Section 5.

2. METHODOLOGY OF STUDY

2.1. Simulation Method

Throughout this study, the discrete element method (DEM) (13) was used to carry out the simulations of granular dampers. In the DEM approach, damping particles and surrounding surfaces of the damper enclosure are modelled as distinct bodies where each of those has a pre-defined geometry and mass. The positions of created bodies are obtained solving the governing equations of motion derived for each of them considering the corresponding residual forces and moments involved. In order to accurately capture contacts and, therefore, compute the forces for constructing the equations of motion, the calculation time step for DEM simulations is typically very small, and depends on material elasticity and density (14).

In DEM, apart from gravitational forces and externally applied loads, the forces acting on each body arise from the interactions between the contacting bodies. The contacts are determined by calculating the smallest distance between two bodies and considering their geometric features. For each detected contact, the contact forces are evaluated according to the implemented theoretical contact approach. In this study, the Hertz-Mindlin contact model was used to compute the normal and tangential elastic forces while the slipping and sliding conditions were determined using the Coulomb friction model between the contacting bodies (15). The inelastic components of collision forces were accounted implementing the approach presented by Tsuji et. al (16).

2.2. Damper Model and Simulation Properties

In this study, Altair EDEM (17) software was used to model and simulate the granular dampers as three-dimensional DEM algorithm. As the aim was to investigate the relative changes in dissipative interaction types in the granular medium under a variety of loading conditions, the granular dampers were modelled as structure independent as shown in Figure 2. In this case, the dynamics of the host structure are not considered.

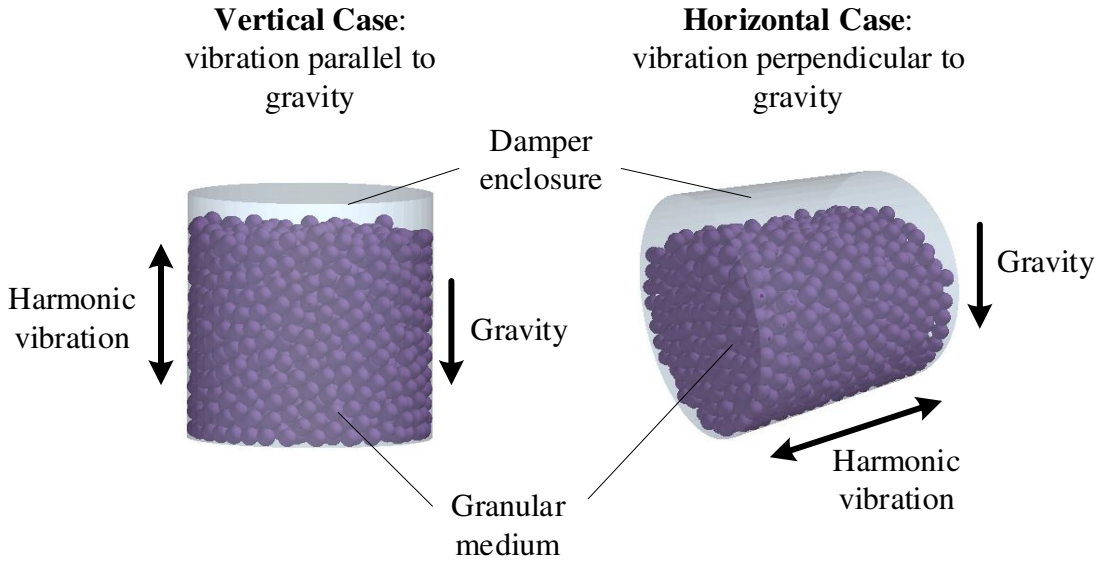

Figure 2: Simulated granular damper model.

The damper enclosure used in the study has a cylindrical geometry whose diameter is 0.04 m. Two different enclosure heights (0.04 m and 0.05 m) were used to investigate the effect of volume fill ratio while maintaining the same total mass of particles. In the simulations, it was assumed that the particles and enclosure are made from the same material whose properties are briefly summarised in Table 1.

Table 1: Material and contact properties used in simulations.

Young's modulus	Poisson's ratio	Density	Coefficient of restitution	Coefficient of friction
3.3 GPa	0.37	1190	0.86	0.52

As shown in Figure 2, two different vibration-to-gravity directional cases were simulated to observe the effect of loading orientation. For each case, the enclosure surfaces were subjected to predefined axial harmonic displacement excitation which can be written as:

$$u(t) = \left(\Gamma g / \omega^2\right) \sin(\omega t) \tag{1}$$

where g is the gravitational acceleration; ω is the vibration frequency (in rad/s); Γ is the non-dimensional acceleration amplitude of harmonic excitation; and t represents time. The investigated frequencies were between 20 Hz and 1024 Hz, and the amplitude range was Γ = 1 to 100 for each simulated damper in this study.

The particles were generated initiating each of them at random positions in the enclosure void, and, afterwards, they were allowed to settle down by the effect of gravity giving a pre-simulation time gap in the simulation set-up lasting 0.2 seconds for each simulation run. Every loading case was simulated by applying defined excitation condition for 8 vibration cycles. As it was found that most transient effects were eliminated after 3 cycles, the last 5 cycles were considered as 'steady-state' and used for computations.

2.3. Dissipated Energy

As DEM provides discrete time-based solution, the total dissipated energy achieved by a granular damper is cumulatively computed at time, t, using:

$$E_{\text{dissipated}}(t) = \sum_{i=1}^{N_{\text{Particle}}} \sum_{j=1}^{N_{\text{Contact},i}(t)} \left\{ \left| \mathbf{F}^{nd}{}_{ij}(t) \cdot \mathbf{v}^{n}{}_{ij}(t) \right| + \left| \mathbf{F}^{td}{}_{ij}(t) \cdot \mathbf{v}^{t}{}_{ij}(t) \right| \right\} \Delta t + E_{\text{dissipated}}(t - \Delta t) \tag{2}$$

where N_{Particle} is the total number of particles; $N_{\text{Contact},i}$ is the total number of contacts involving particle i; $\mathbf{F}^{nd}{}_{ij}$ and $\mathbf{F}^{td}{}_{ij}$ are the dissipative forces in normal and tangential directions, respectively; $\mathbf{v}^{n}{}_{ij}$ and $\mathbf{v}^{t}{}_{ij}$ are the corresponding relative velocities and Δt is the time step.

As the aim is to examine the dissipative interaction types, the relative contributions of different interaction types in the total dissipated energy need to be determined. For example, in the next section of this paper, dissipative contributions of particle-particle and particle-enclosure contacts are investigated along with phase maps. If $N_{\text{Contact},i}$ counts only particle-particle contacts (i.e., excludes particle-enclosure surface contacts), the total dissipated energy from only particle-particle (PP) contacts,

$E^{PP}_{dissipated}$, is obtained via the above equation. The remaining dissipated energy is caused by particle-enclosure surface (PW) contacts, and it can be found as: $E^{PW}_{dissipated} = E_{dissipated} - E^{PP}_{dissipated}$.

3. RELATION BETWEEN DISSIPATIVE INTERACTION TYPE AND PHASE MAP

3.1. Overview of observed motional phases

Using simulation footage, 7 different motional phases in the vertical case ('solid-like', 'local fluidisation', 'global fluidisation', 'Leidenfrost effect', 'buoyancy convection', 'transitions' 'bouncing bed') and 4 different phases in the horizontal case ('partial fluidisation', 'fluidisation/convection', 'convection', 'bouncing bed') were identified within the investigated loading range. As much as possible, phase names were kept consistent with the literature terminologies and motional definitions (7,18–21).

There are basically 4 fundamental motional behaviours that determine these phases. 'Solid-like' behaviour indicates insignificant relative motions amongst particles and between particles and enclosure. This motion type leads negligibly low energy dissipation in granular damping (10). 'Fluidisation' represents the relative motion of particles maintaining their approximate relative positions and existing contacts at the end of each vibration cycle. The fraction of fluidised particles in a granular medium determines the fluidisation-based phases: the local fluidisation, the global fluidisation, the partial fluidisation and fluidisation/convection. These fluidisation-based phases are considered as the effective granular damping phases for wide frequency range applications. 'Convection' means that the particles move in patterns and change their contacts and as a result yields low energy dissipation efficiency. The names including the Leidenfrost effect, the buoyancy convection and the convection phases depend on the pattern that the particles follow in this motion type. These convection-based phases yield low granular energy dissipation performance as the large portion of particles shows convection motion (10). The bouncing bed (sometimes called two-sided bouncing bed) has a different motional analogy than solid-fluid-convection motions and exhibits two collective collisions of granular medium as a packed mass with two ends of enclosure. This motional phase provides very efficient granular energy dissipation – particularly vicinity of the bouncing bed onset amplitude (10,22).

3.2. Vertical Case

In vertical excitation, the PP dissipation contribution fractions and the observed motional phases are mapped along the vibration amplitude and frequency in Figure 3 for two different particle sizes. As the motional behaviour of granular medium is strongly governed by volume fill ratio, the presented phase maps in Figure 3 are nearly same – only the phase boundaries slightly differ. For example, the convection-based motion phases are observed at lower vibration amplitudes for the larger particle as they de-compact and change position more easily. This is because there are fewer restrain forces acting on a particle due to decrease in the coordination number.

It can be seen from Figure 3 that the PP dissipation is the dominant dissipative interaction over PW dissipation for each excitation condition. However, the fraction of PP dissipation can be seen to change depending on the operating motional phase and particle size.

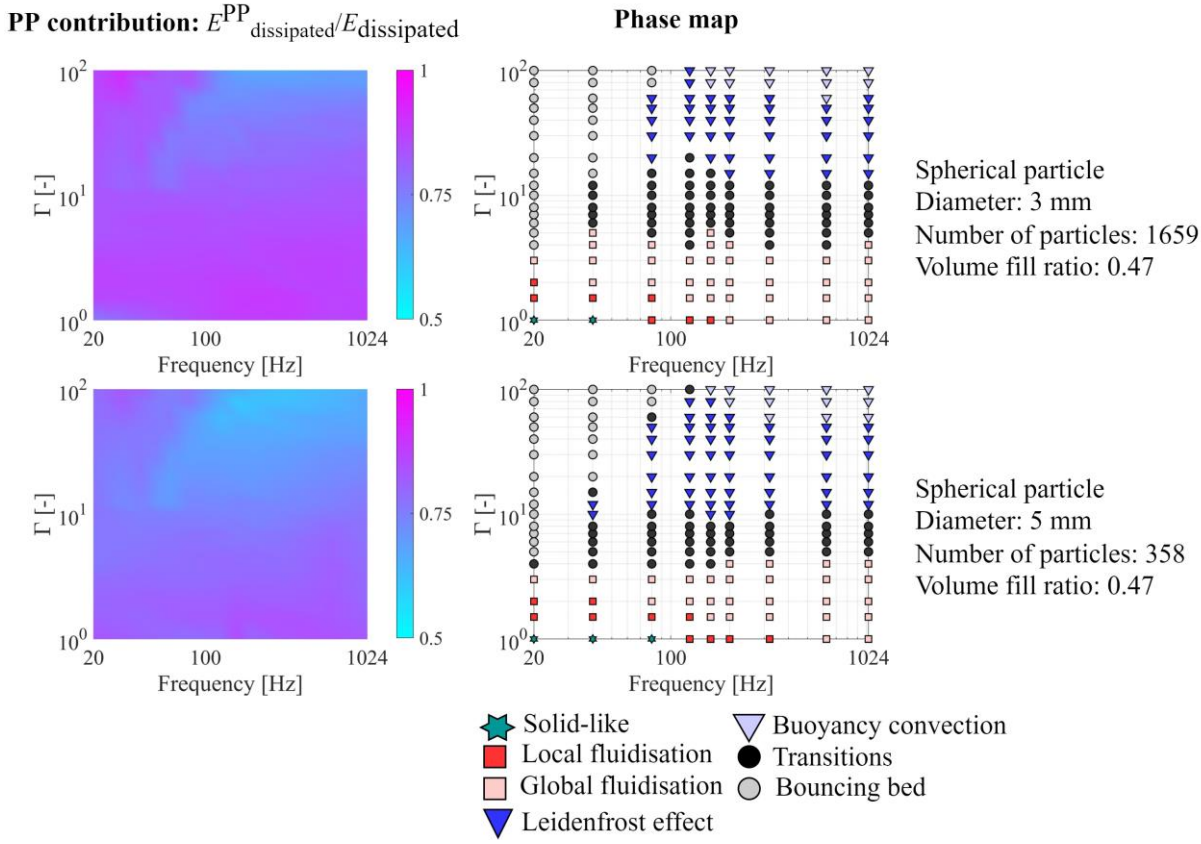

Figure 3: PP dissipation contribution and phase maps in the vertical case.

Comparing the PP contribution of two different sized particles in Figure 3, it is apparent that the overall PP contribution reduces as the particle size grows as the number of particles decreases. In order to observe solely the effect of operating motional phase, the relative PP dissipation contributions can be used.

$$\left(\frac{E^{PP}_{dissipated}}{E_{dissipated}}\right)_{normalised} = \frac{E^{PP}_{dissipated}/E_{dissipated} - \min\left\{E^{PP}_{dissipated}/E_{dissipated}\right\}}{\max\left\{E^{PP}_{dissipated}/E_{dissipated}\right\} - \min\left\{E^{PP}_{dissipated}/E_{dissipated}\right\}} \tag{3}$$

The normalised PP contribution distributions are shown in Figure 4 along with the corresponding phase maps for different particle types and volume fill ratios. In these graphs, it can be seen that the convection-based phases are distinguishable from the other phases as they produce relatively very low PP dissipative contribution. There is a visible inclined ridge-like sudden change in the PP normalised contribution that separates the bouncing bed phase and the Leidenfrost effect or the buoyancy convection, and there is a nearly horizontal boundary which shows the intersection between the transition phase and the Leidenfrost effect. This recognisable difference between the convection-based phases and the other phases is caused by the fundamental definition of particle convection motion. It should be also noticed in Figure 4 that the PP dissipation contribution further decreases when the buoyancy convection phase is initiated by growing the vibration amplitude.

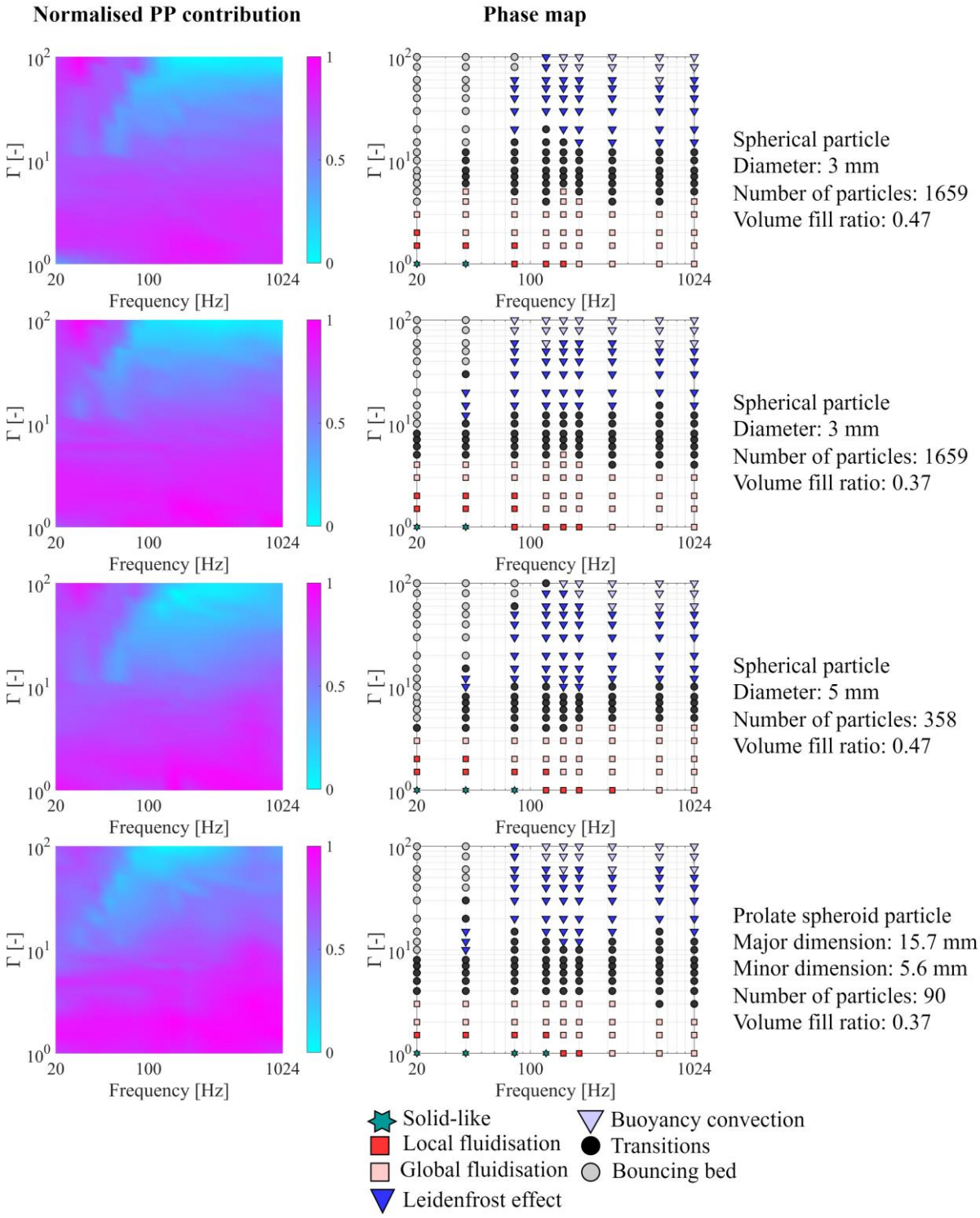

Figure 4: Normalised PP dissipation contribution and phase maps in the vertical case.

Since the particle size does not significantly affect the phase map (as long as there are sufficient particle layers), the normalised PP dissipation contribution distributions for 3 mm and 5 mm particles are very similar. Note that the approximately horizontal boundary between the Leidenfrost effect and

the transition phase reduces as the particle size grows, and it can be observed comparing the related normalised PP contribution maps.

Figure 4 shows that the volume fill ratio changes the inclined boundary of relatively low PP dissipation contribution. As this boundary corresponds to the bouncing bed – the convection-based phases intersection, it indicates that the convection-based region widens as the volume fill ratio decreases within the same investigated excitation range. This inclined bouncing bed ridge can also be determined analytically (7,10,23).

As a different particle shape (i.e., a prolate spheroid), the normalised PP dissipation contribution map again displays the convection-based phase region. It should be noted that even though the particle shape does not affect the phase map much as shown in Figure 4, the particle shape can change the phase transition regions (24).

The other phases could not be determined using the normalised PP dissipative contributions as can be seen from Figure 4. However, as these results encourage, it is thought that it would be possible in a future work which calculates the approximate boundary limits of each particular motional phases.

3.3. Horizontal Case

For the horizontal excitation, the normalised PP dissipative contribution and the phase map are presented in Figure 5. As can be seen from this figure, the normalised PP contribution can still reflect the region in which the convection-based motions are observed. By comparing Figure 4 and Figure 5 it can be noted that the PP contribution maps are quite similar even though the motional behaviours, and therefore the phase names differ. It is because of the similarity of principal motion types in both excitation cases: solid-like, fluidisation, convection, and collective collision.

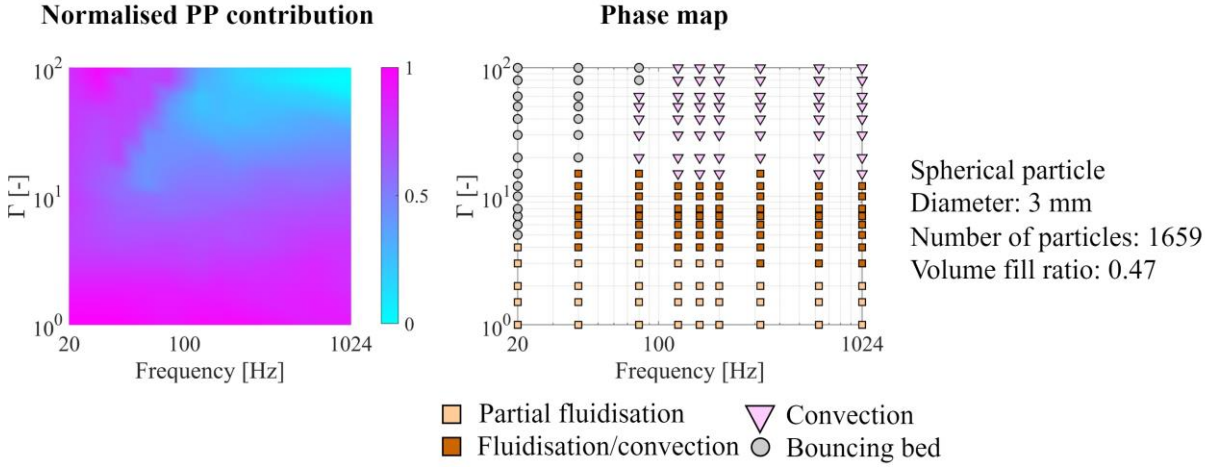

Figure 5: Normalised PP dissipation contribution and phase map in the horizontal case.

4. ON THE MOST EFFECTIVE GRANULAR ENERGY DISSIPATION MOTION TYPES

As mentioned before, there are mainly two different fundamental motion types where the granular energy dissipation is most efficient: collective collision (i.e., the bouncing bed) and fluidisation behaviour. As shown looking at the relevant arrows in Figure 6 and discussed before, the granular dissipation effectiveness decreases from which the dissipation is maximised in these particular motion types towards larger vibration amplitudes.

As the fundamental factors that affect these motion types are different, the explanations of dissipative efficiency reduction are also different for these motions. In the bouncing bed phase, the granular medium becomes more closely packed as the vibration amplitude increases. This results in a reduction in the rate of dissipated power to the vibration input power. On the other hand, as the vibration amplitude grows, zones of fluidisation within the granular medium are gradually replaced by convective behaviour. This causes the granular energy dissipation efficiency reduction through fluidisation-convection path. Here, the effects of the mentioned dissipative efficiency reductions are briefly investigated by means of the relative contributions of different dissipative interaction types.

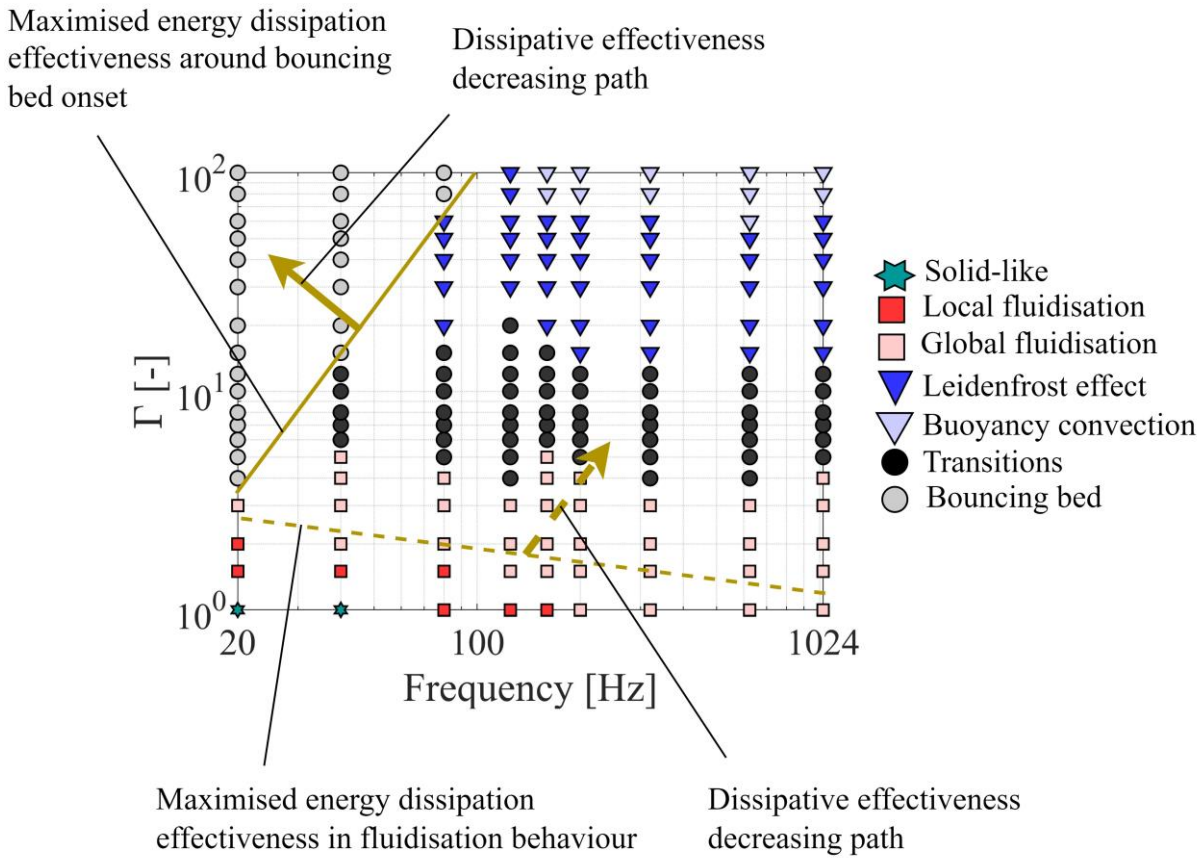

Figure 6: Granular energy dissipation effectiveness reduction paths on phase map.

4.1. Bouncing Bed Phase

Figure 7 shows the fractions of PP dissipative contribution and frictional dissipative contribution in the total dissipated energy for varying vibration amplitude at 20 Hz and 40 Hz. Note that the frictional dissipation contribution is calculated considering only the frictional forces in Equation 2 as the dissipative force. The remaining fraction of total dissipated energy (counterpart of the frictional contribution) arises from the inelastic collisions.

It can be seen by comparing Figure 6 and Figure 7 that both investigated dissipative contribution types become steadier in the bouncing bed phase as the granular medium motional behaviour is in a regular pattern within a vibration cycle. Before the bouncing bed is initiated, there are visible fluctuations as the granular medium shows fluidised and convection motions.

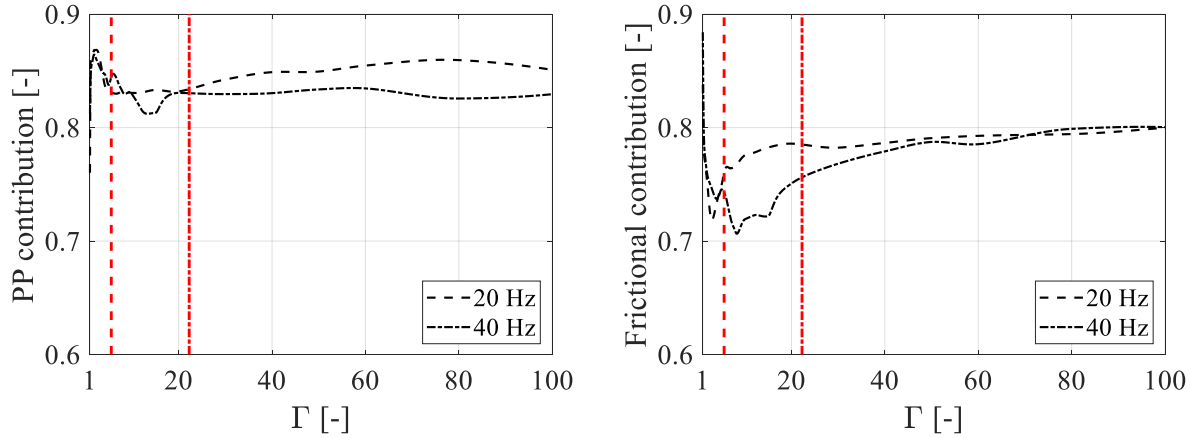

Figure 7: Fractions of PP and frictional dissipative contributions of 3 mm spherical particles for 0.47 of volume fill ratio (the vertical lines correspond to the approximate onset amplitudes of bouncing bed phase where the energy dissipation effectiveness is maximised at the shown frequencies, note that the right sides of vertical lines indicate the bouncing bed phase region).

Figure 7 demonstrates that the frictional dissipation is much greater than the inelastic collisional loss in the bouncing bed phase. Although the bouncing bed produces two intensive collective collisions with the enclosure ends in a vibration cycle, the sliding activities within the granular medium during these impacts dominate the energy dissipation. It is interesting that the frictional dissipation particularly approaches 80% for both investigated frequencies as the granular medium form more compact structure with increasing amplitude. It indicates that there is a maximum level for the compactness (that the particles can be compressed). This limitation level is also 80% for different volume fill ratios and slightly decreases with increasing particle size – e.g., 77% for 5 mm spherical particles.

4.2. Fluidisation Motion

Figure 8 shows the fractions of PP and frictional dissipative contributions in the total dissipated energy along a range of vibration amplitude for some vibration frequencies – showing solid-fluidisation-convection path (see Figure 6 to follow). Note that the occurrence density of convection motions increases towards the transition phase.

For the smaller vibration amplitudes than $\Gamma = 3$, the PP contribution is generally larger than 86% and maximised within this amplitude range. This amplitude range is attributed to the densifying of fluidisation phase within the granular medium. Therefore, the most efficient granular energy dissipation apart from the bouncing bed phase is observed around $\Gamma = 2$-3 along a wide range of frequency, where the fluidisation motion is maximised. For $\Gamma > 3$, the fluidisation density decreases with increasing amplitude, and this starts yielding apparent reduction in the PP dissipation contribution as can be seen in Figure 8 – e.g., approximately 82% for $\Gamma = 10$ and it was found that this ratio can reduce to 67% in the buoyancy convection. It was not given in here, but the fraction of PP dissipative contribution is not affected by the volume fill ratio as it does not affect fluidisation and convection motions.

Regardless of motional phase, the frictional contribution reduces as the vibration amplitude grows and generally increases with increasing frequency.

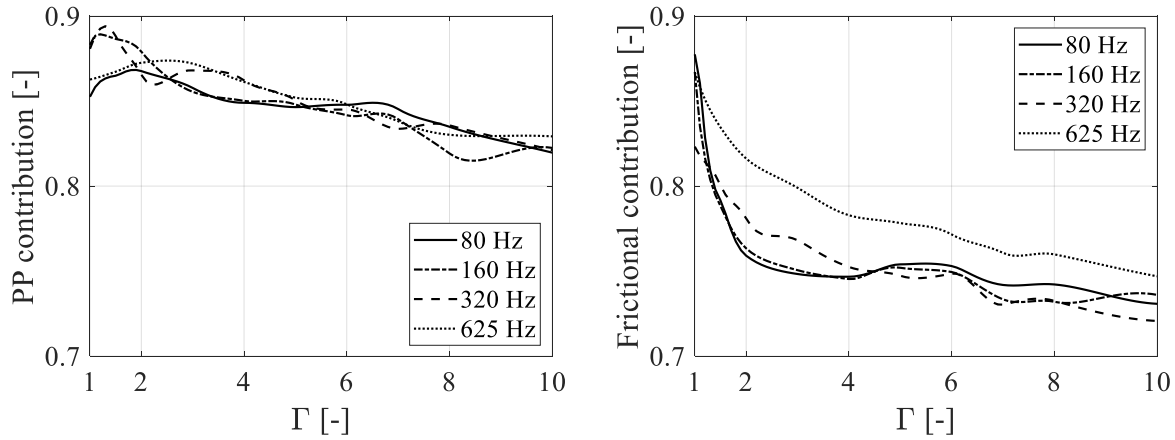

Figure 8: Fractions of PP and frictional dissipative contributions of 3 mm spherical particles for 0.47 of volume fill ratio.

5. CONCLUSIONS

The purpose of this study was to provide a simulation-based approach which investigates the relative importance of dissipative interaction types in different operating motional phases of a granular damper. This study was caried out exciting the particulate system by a variety of vibration amplitude and frequency in DEM environment. In this way, it was examined whether a granular phase map can be estimated from the expected dissipative interaction behaviour in a particular motional phase. It was found that the relative changes in the dissipative contributions of interaction types can be attributed to the observed motional phase regardless of particle size, volume fill ratio, particle shape and vibration-to-gravity directional orientation. From the particle-particle interaction contribution fraction of the total dissipated energy, the convection-based motions, in which the granular energy dissipation effectiveness is low, were found as detectable since they produced apparently less particle-particle dissipative contacts than the other phases. As a result, such physical interpretation-based approach can be extended to develop an index to predict the granular phase map without performing time consuming visual observations on simulations or experiments. Also, a particular investigation was conducted on the bouncing bed and fluidisation motions where the granular energy dissipation performance can be optimised to observe the relative changes in the dissipative interaction contributions as the dissipation performance decreases towards large vibration amplitudes in these motion types.

6. REFERENCES

1. Veeramuthuvel P, Sairajan KK, Shankar K. Vibration suppression of printed circuit boards using an external particle damper. *Journal of Sound Vibration*, **366**, 98–116 (2016).
2. Xu Z, Yu Wang M, Chen T. A particle damper for vibration and noise reduction. *Journal of Sound Vibration*, **270(4–5)**, 1033–40 (2004).
3. Duvigneau F, Koch S, Woschke E, Gabbert U. An effective vibration reduction concept for automotive applications based on granular-filled cavities. *Journal of Vibration and Control*, **24(1)**, 73–82 (2018).
4. Moore JJ, Palazzolo AB, Gadangi R, Nale TA, Klusman SA, Brown G V., et al. A forced response analysis and applicationof impact dampers to rotordynamic vibration suppression in a cryogenic environment. *Journal of Vibration and Acoustics*, **117(3)**, 300–10 (1995).

5. Shah BM, Pillet D, Bai XM, Keer LM, Jane Wang Q, Snurr RQ. Construction and characterization of a particle-based thrust damping system. *Journal of Sound Vibration*, **326(3–5)**, 489–502 (2009).
6. Fowler BL, Flint EM, Olson SE. Design methodology for particle damping. *Proceedings of SPIE 4331, Smart Structures and Materials 2001: Damping and Isolation*. pp. 186–97. Newport Beach, California, USA, July 2001.
7. Meyer N, Seifried R. Toward a design methodology for particle dampers by analyzing their energy dissipation. *Computational Particle Mechanics*, **8**, 681-699 (2020).
8. Wong CX, Daniel MC, Rongong JA. Energy dissipation prediction of particle dampers. *Journal of Sound Vibration*, **319(1–2)**, 91–118 (2009).
9. Salueña C, Pöschel T, Esipov SE. Dissipative properties of vibrated granular materials. *Physical Review E*, **59(4)**, 4422–5 (1999).
10. Terzioglu F, Rongong JA, Lord CE. Motional phase maps for estimating the effectiveness of granular dampers. *Mechanical Systems and Signal Processing*, **(Submitted)** (2022).
11. Eshuis P, van der Weele K, van der Meer D, Bos R, Lohse D. Phase diagram of vertically shaken granular matter. *Physical Fluids*, **19(12)** (2007).
12. Zhang K, Zhong H, Chen T, Kou F, Chen Y, Bai C. Dissipation behaviors of granular balls in a shaken closed container. *Mechanical Systems and Signal Processing*, **172** (2022).
13. Cundall PA, Strack ODL. A discrete numerical model for granular assemblies. *Geotechnique*, **29(1)**, 47–65 (1979).
14. Lommen S, Schott D, Lodewijks G. DEM speedup: Stiffness effects on behavior of bulk material. *Particuology*, **12(1)**, 107–12 (2014).
15. Di Renzo A, Di Maio FP. Comparison of contact-force models for the simulation of collisions in DEM-based granular flow codes. *Chemical Engineering Science*, **59(3)**, 525–41 (2004).
16. Tsuji Y, Tanaka T, Ishida T. Lagrangian numerical simulation of plug flow of cohesionless particles in a horizontal pipe. *Powder Technology*, **71(3)**, 239–50 (1992).
17. Altair Engineering Inc. EDEM 2021.1. (2021).
18. Zhang K, Chen T, Wang X, Fang J. Rheology behavior and optimal damping effect of granular particles in a non-obstructive particle damper. *Journal of Sound Vibration*, **364**, 30–43 (2016).
19. Yin Z, Su F, Zhang H. Investigation of the energy dissipation of different rheology behaviors in a non-obstructive particle damper. *Powder Technology*, **321**, 270–5 (2017).
20. Pöschel T, Schwager T, Salueña C. Onset of fluidization in vertically shaken granular material. *Physical Review E*, **62(1 B)**, 1361–7 (2000).
21. Salueña C, Pöschel T. Convection in horizontally shaken granular material. *European Physical Journal E*, **1(1)**, 55–9 (2000).
22. Sack A, Windows-Yule K, Heckel M, Werner D, Pöschel T. Granular dampers in microgravity: sharp transition between modes of operation. *Granular Matter*, **22(2)**, 1–6 (2020).
23. Sack A, Heckel M, Kollmer JE, Zimber F, Pöschel T. Energy dissipation in driven granular matter in the absence of gravity. *Physical Review Letter*, **111(1)**, 1–5 (2013).
24. Terzioglu F, Rongong JA, Lord CE. The dissipative characteristics of oblate particles in granular dampers. *Proceedings of the International Conference on Structural Dynamic (EURODYN2020)*, pp. 4851–66. Athens, Greece, November 2020.